ARTICLE

Effects of Traps on Photo-induced Interfacial Charge Transfer of Ag-TiO_2: Photoelectrochemical, Electrochemical and Spectroscopic Characterizations

Zhi-Hao Liang, Jia-Zheng Wang, Dan Wang, Jian-Zhang Zhou*, De-Yin Wu

State Key Laboratory of Physical Chemistry of Solid Surfaces and College of Chemistry and Chemical Engineering, Xiamen University, Xiamen, 361005, Fujian, China

Abstract

In the field of metal-semiconductor composites based plasmon-mediated chemical reactions, a clear and in-depth understanding of charge transfer and recombination mechanisms is crucial for improving plasmonic photocatalytic efficiency. However, the plasmonic photocatalytic reactions at the solid-liquid interface of the electrochemical systems involve complex processes with multiple elementary steps, multiple time scales, and multiple controlling factors. Herein, the combination of photoelectrochemical and electrochemical as well as spectroscopic characterizations has been successfully used to study the effects of traps on the photo-induced interfacial charge transfer of silver-titanium dioxide (Ag-TiO_2). The results show that the increase of surface hydroxyl groups may be the key reason leading to the increase of traps after the Ag deposition on the surface of TiO_2. The increased traps of Ag-TiO_2, including deep and shallow traps, subsequently lead to the quenching of fluorescence and the reduction of photocurrent in the UV region. But the enhanced trap recombination may also prolong the lifetime of carriers. The modulation of traps is bound to affect the interfacial charge transfer, and thus, change the amount and lifetime of hot carriers, which can be exploited to manipulate the molecular reactions at the Ag surface. Our work highlights the importance of traps at metal-semiconductor electrodes that may help utilize the hot carriers in plasmonic mediated chemical reactions.

Keywords: Plasmonic; Silver-titanium dioxide; Trap state; Charge transfer; Photoelectrochemical characterization

1. Introduction

Under light excitation, a collective oscillation phenomenon, which is called localized surface plasmon resonance (LSPR), will occur when the vibration frequency of free electrons on the surface of noble metal nanoparticles (Au, Ag, Cu, etc.) matches the frequency of the excitation light. After the plasmons of noble metal nanoparticles (NPs) were excited, the hot carriers generated by non-radiative relaxation of the plasmons may be transferred to the adsorbed molecules through the interface, thereby inducing the interfacial oxidation or reduction reactions [1−3]. Compared with traditional photocatalytic reactions, plasmon-mediated chemical reactions (PMCR) have the advantages of low energy input, high selectivity, and mild reaction conditions [4]. However, hot carriers with higher energy tend to have shorter lifetime. The lifetime of hot carriers generated by plasmonic relaxation of metal NPs is generated on the femtosecond-picosecond time scale, while the time scale of interfacial reactions, especially electrochemical reactions, is usually in microsecond or even longer [5]. Therefore, most of the hot carriers are consumed by recombination before reacting with adsorbed molecules on the surface, which leads to the low photochemical energy conversion efficiency of metal NPs. The Schottky barrier at the metal-semiconductor interface is formed when semiconductors such as TiO_2 or ZnO_2 are combined with metal NPs. The Schottky barrier can

Received 10 August 2022; Received in revised form 9 September 2022; Accepted 14 September 2022
Available online 15 September 2023

* Corresponding author, Jian-Zhang Zhou, Tel: (86-592)2189663, E-mail address: jzzhou@xmu.edu.cn.

https://doi.org/10.13208/j.electrochem.2208101
1006-3471/© 2023 Xiamen University and Chinese Chemical Society. This is an open access article under the CC BY-NC license (http://creativecommons.org/licenses/by-nc/4.0/).

separate the hot electron-hole pairs with energy higher than the barrier and prolong their lifetime [5]. Hence, the construction of metal-semiconductor composite is considered to be one of the hopeful solutions to improve the utilization efficiency of hot carriers [6−8].

Among noble metal NPs, Ag NPs have significant advantages in light scattering properties, near-field enhancement, and economical efficiency. However, the high carrier recombination efficiency and poor chemical stability limit their wide application. TiO_2, as one of the most widely used wide band-gap semiconductors in photocatalysis, has good photochemical stability and electron transport properties. The combination of Ag and TiO_2 can improve the stability of Ag NPs and also prolong the lifetime of carriers. In recent years, Ag-TiO_2 composite has been widely exploited in the fields of water splitting [6], CO_2 reduction [9], and degradation of organic pollutants [10,11]. However, most of the researches on Ag-TiO_2 composites were from the perspectives of enhancing the light absorption of semiconductor and improving the efficiency of photocatalytic reactions that occurred mostly on semiconductors, while less attention was paid to PMCR at the Ag surface in the composites. It is obvious that the behaviors of photogenerated carriers (including generation, separation, transfer, and recombination) are crucial to improving the efficiency of photocatalytic reactions. Thus, more in-depth investigations are needed to find out how the electronic and structural properties of TiO_2 affect the charge transfer between Ag and TiO_2, and then the PMCR on Ag. Furthermore, the surface defects of TiO_2 usually result in different intra-band gap states and traps. The traps are distributed within the band gap of the semiconductor which can be divided into deep and shallow traps in terms of their energy. The deep trap states may impede carrier transfer. In contrast, shallow traps may contribute to carrier transfer. It is essential to understand the chemical nature of these traps and their effects on interfacial charge transfer in metal-semiconductor composites so that they could be manipulated for a PMCR application.

Previous studies in the interfacial charge transfer mechanism of the plasmonic-semiconductor composite were mainly conducted at the gas-solid interface by using femtosecond transient absorption spectroscopy [12]. Thus, the interfacial charge transfer mechanism of solid-liquid interface and photoelectrochemical system operating in solution was not well established. Part of the reason was that solid-liquid interfaces in photoelectrochemical systems are more complex than gas-solid interfaces, which brings difficulties to the utilization of transient absorption spectroscopy. But knowledge of the charge transfer mechanism at the solid-liquid interface is important for in-depth understanding and further utilization of PMCR. Since the generation and change of photoelectrochemical response (photocurrent and photopotential) are closely related to the transport and recombination behaviors of carriers, photoelectrochemical methods seem to be one of the effective methods to study interfacial charge transfer [13].

Herein, the Ag-TiO_2 NPs were synthesized and the interfacial charge transfer mechanism was investigated in detail using photoelectrochemical, electrochemical, and spectroscopic methods. The traps of Ag-TiO_2 electrode were investigated by photoluminescence spectroscopy and chronoamperometry. The interfacial transfer and recombination behaviors of photogenerated carriers of Ag-TiO_2 were studied by transient photocurrent and photopotential methods. Finally, the charge transfer mechanism is proposed and the effects of traps of the Ag-TiO_2 composite are discussed, which may provide insight into the photocatalytic processes of the plasmonic metal-semiconductor composite system.

2. Experimental

2.1. Chemical reagents and instrumentations

Chemical reagents of $AgNO_3$, polyvinylpyrrolidone (PVP, K30), $NH_3 \cdot H_2O$, H_2O_2 (30%), and $NaClO_4$ were purchased from Shanghai Chemical Reagent Company. $TiCl_4$ (99.6%) was purchased from Alfa Aesar. All the chemicals were used as received without further purification. Milli-Q water (18.2 MΩ cm) was used in all experiments.

Scanning electron microscopic (SEM) images were acquired with HITACHI S-4800 and the average size of the NPs was obtained by individually measuring at least 100 NPs. Transmission electron microscopic (TEM) and high-resolution transmission electron microscopic (HRTEM) images were collected using FEI-tecnai F30. X-ray powder diffraction (XRD) measurements were performed in Rigaku Ultima IV diffractometer with Cu Kα radiation ($\lambda = 1.5417$ Å). X-ray photoelectron spectroscope (XPS) with monochromatized Al K_α radiation (VG, Physical Electrons Quantum 2000 Scanning ESCA Microprobe) was used to obtain the surface chemical composition and electronic state. The light absorption of samples was measured using a UV−Vis/NIR spectrophotometer

(Varian, Cary 5000). Photoluminescence (PL) spectra were acquired using a Hitachi F-7000 fluorescence spectrophotometer with a Xenon lamp as the excitation source (λ_{ex} = 375 nm).

2.2. Preparations of TiO_2 and Ag-TiO_2 NPs

Ag-TiO_2 NPs were synthesized in two steps [14,15]. Fig. 1 shows the schematic representation for the syntheses of TiO_2 and Ag-TiO_2 NPs. Initially, the TiO_2 NPs were synthesized by a hydrothermal process. Under vigorous stirring, $NH_3 \cdot H_2O$ (1 mol·L^{-1}) solution was added to ice-cold water (50 mL) containing Ti^{4+} solution (0.005 mol·L^{-1}) to retain its pH at 9 and kept in an oven at 90 °C for 3 h. Later, the obtained precipitate was thoroughly washed with water and dispersed in 100 mL deionized water. H_2O_2 (30%, 100 mL) was added to the above content to obtain the orange-yellow colored peroxotitanic acid (PTA) solution. Then, the mixture was transferred into a Teflon-lined autoclave and kept in an oven, and heated at 140 °C for 24 h. Finally, the anatase TiO_2 sol was obtained.

The prepared TiO_2 sol (25 mL) was washed and dispersed in 50 mL of deionized water. The pH was adjusted to 9 with diluted NaOH (1 mol·L^{-1}) solution. Then, PVP (0.8 g) was sequentially injected under vigorous stirring. Finally, $AgNO_3$ (10 mmol·L^{-1}, 11.7 mL) solution was slowly added to the TiO_2 solution by a stepper. Here, PVP serves as a surface stabilizer and reducing agent. PVP adsorbs on the surface of Ag particles and slowly reduces Ag^+ to Ag NPs under hydrothermal condition. After the addition of $AgNO_3$, the reaction was carried out at 90° for 8 h. Then the obtained Ag-TiO_2 NPs were kept aside to cool at room temperature.

2.3. Fabrications of TiO_2 and Ag-TiO_2 NPs electrodes

F-doped tin oxide (FTO) substrates were previously cleaned in a mixture of acetone (10 mL), 2-propanol (10 mL) and deionized water (10 mL) using ultrasonication for 1 h. Previously synthesized TiO_2 and Ag-TiO_2 NPs (2 mL) were centrifugally washed with deionized water and concentrated to 200 μL, then drop-coated on the FTO surface to form a dense membrane electrode (the area of the FTO with NPs was about 1 cm × 1 cm).

2.4. Electrochemical and photoelectrochemical measurements

Electrochemical and photoelectrochemical experiments were carried out using a CHI630A electrochemical workstation (CH Instruments, China) with a three-electrode system: the as-prepared Ag-TiO_2 or TiO_2 electrode acted as the working electrode, a piece of 1 cm × 1 cm platinum sheet as the counter electrode, and a saturated Ag/AgCl electrode as the reference electrode. 0.5 mol·L^{-1} $NaClO_4$ was used as the electrolyte. Potential step chronoamperometric (CA) tests were carried out in dark condition. The electrode was first polarized at 0.25 V for 30 s, then the potential was stepped immediately to a lower potential and the transient current was recorded. The photocurrent experiment was carried out using the amperometric current-time (*i-t*) technique and the light exposure interval was set to be 10 s. The photopotential of the nano-electrode was recorded by the open circuit potential (OCP) technique, and the electrode was first equilibrated

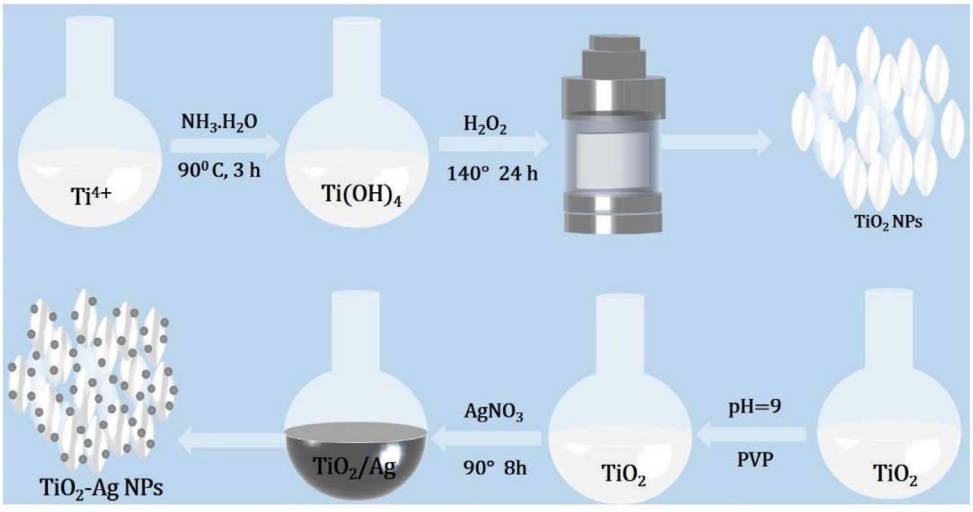

Fig. 1. Schematic diagram for the syntheses of TiO_2 and Ag-TiO_2 NPs.

in the dark for 100 s, then the potential was recorded under intermittent illumination. The charge recombination process was recorded after turning off the light.

3. Results and discussion

3.1. Crystal structure and morphology characterization of NPs

Fig. 2a shows the XRD patterns of TiO_2 and Ag-TiO_2 NPs. Among the diffraction peaks, the peaks located at 25.2°, 37.8°, 47.8°, 54.3°, and 61.6° are ascribed to anatase TiO_2 (101), (004), (200), (105), and (213) planes (#21−1272), respectively. The peaks at 37.8° and 44.5° are assigned to Ag (111) and (200) planes (#04−0783), respectively, indicating that Ag exists in an elemental form in Ag-TiO_2 NPs. Except for the diffraction peaks of SnO_2 from the FTO substrate, no other unattributed diffraction peaks were detected. In the Ag-TiO_2 composites, the peaks of anatase TiO_2 at 25.2°, 54.3°, 69.5°, and 70.3° are weaker than those of TiO_2, which may be due to the covering and shielding effects of Ag. Besides, no shifts in the positions of diffraction peaks are observed. This means that Ag is not doping in the TiO_2 lattice but is mainly deposited on the surface of TiO_2 [16].

XPS analyses were conducted to further explore the elemental composition and valence state of TiO_2 and Ag-TiO_2 NPs. Compared with the XPS pattern of TiO_2, the presence of the Ag peak in Ag-TiO_2 NPs further demonstrated that Ag had successfully located at the surface of TiO_2 (Fig. 2b). The element content ratio of Ti and O is about 1:2 in pristine TiO_2 NPs, while 1:2.5 in the Ag-TiO_2 NPs. Then a high-resolution spectral analysis of each element was performed, as shown in Fig. 2c, the O 1s peak can be fitted into two peaks that are ascribed to the Ti−O bond (529.9 eV) and the surface hydroxyl oxygen (531.5 eV). Compared with the pristine TiO_2, the content of hydroxyl oxygen (the green area) for the Ag-TiO_2 NPs increases obviously, indicating that the improving oxygen content can be assigned to the improving hydroxyl oxygen on the surface of Ag-TiO_2 NPs. The small displacement for the peaks of pristine TiO_2 and Ag-TiO_2 NPs indicates the electron transfer process between Ag and TiO_2. The Ag 3 d

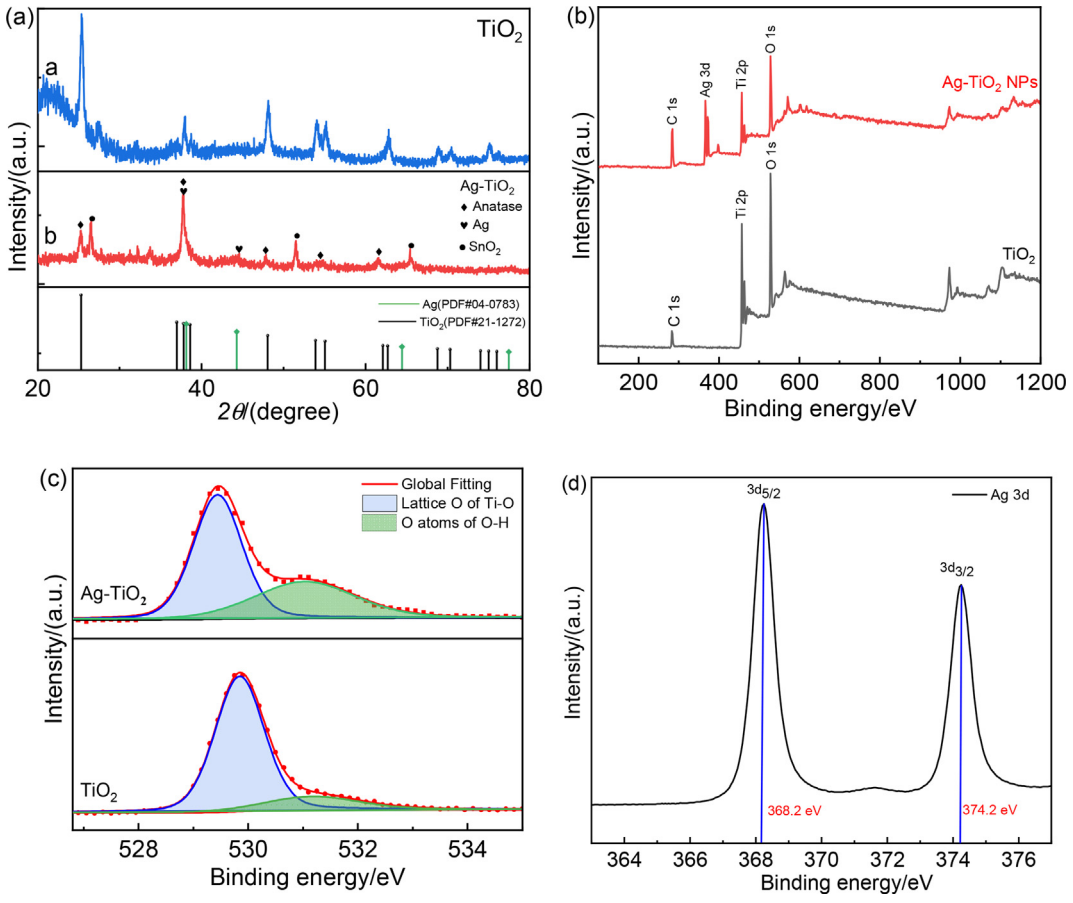

Fig. 2. (a) XRD patterns of TiO_2 and Ag-TiO_2 NPs; (b) XPS survey spectra of TiO_2 and Ag-TiO_2; high-resolution XPS spectra of (c) O 1s and (d) Ag 3 d.

peaks are located at 368.2 eV and 374.2 eV with an energy difference of 6 eV. The position and energy difference of these two peaks also demonstrate that Ag exists in an elemental (Ag^0) form in the Ag-TiO_2 NPs [17].

The morphologies of TiO_2 and Ag-TiO_2 NPs were analyzed by SEM and TEM. As shown in Fig. 3a, the pristine TiO_2 NPs display spindle shape with uniform morphology. After the Ag NPs were loaded on the surface of TiO_2, there is no significant change in the morphology of TiO_2, and Ag NPs are distributed on the surface of TiO_2 in spherical form (Fig. 3b and c). The length and short diameter of TiO_2 NPs were about 49 nm and 25 nm, respectively, and the average size of Ag NPs was about 6 nm. As displayed in Fig. 3d, the lattice spacing values of 0.234 nm and 0.354 nm determined by HRTEM correspond to the Ag (111) plane and TiO_2 (101) plane, respectively, indicating that Ag^0 had successfully attached to the surface of TiO_2 [18], which is also consistent with the XRD and XPS data.

3.2. Optical properties of TiO_2 and Ag-TiO_2 NPs

The UV−Vis absorption spectra of synthesized TiO_2 and Ag-TiO_2 NPs are displayed in Fig. 4a. The onset wavelength of the TiO_2 absorption spectrum at about 385 nm corresponds to the fundamental absorption of anatase TiO_2. The Ag-TiO_2 NPs exhibited a broader absorption in the visible light region with a peak near 420 nm, which may be attributed to the SPR effect of Ag. However, the absorbance of composite samples decreases in the region of 200−350 nm, which is due to the coverage with Ag NPs. The band gaps of TiO_2 and Ag-TiO_2 NPs were calculated using the Tauc formula (Fig. S1), which are 3.20 eV and 2.87 eV, respectively. The Ag NPs were not doping into the lattice but deposited on the surface of anatase TiO_2 according to the previous results of XRD and morphology analyses. Therefore, the narrowing band gap of Ag-TiO_2 NPs can be attributed to changes in surface states, which can form quasi-continuous defect energy levels between the CB and VB of TiO_2. The calculated band gap of Ag-TiO_2 NPs is also called the pseudo-band gap.

Fig. 4b presents the photoluminescence (PL) spectra of TiO_2 and Ag-TiO_2 NPs excited at 385 nm. Because the Ag NPs cannot result in new fluorescence phenomena, the PL peak positions of Ag-TiO_2 and TiO_2 are similar, showing two main PL emission peaks located at 501 nm and 607 nm, respectively. However, the PL peak intensities of Ag-TiO_2 are

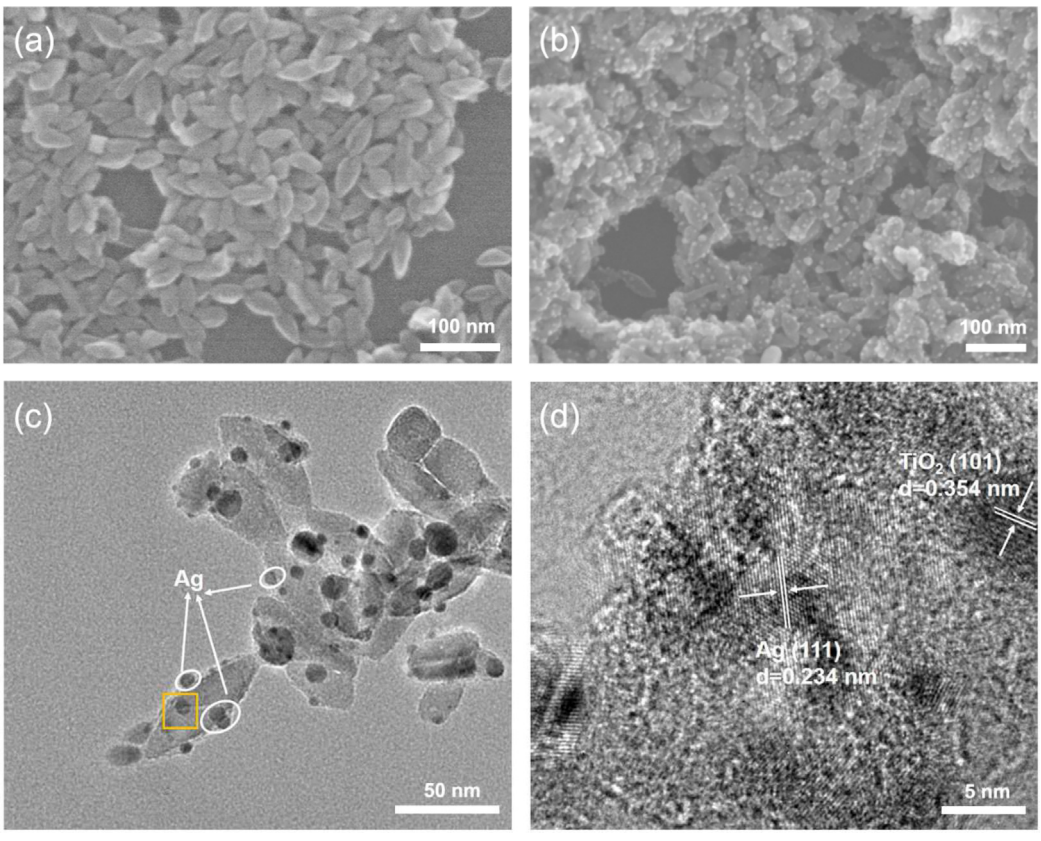

Fig. 3. SEM images of (a) TiO_2 NPs and (b) Ag-TiO_2 NPs; (c) TEM and (d) HRTEM images of Ag-TiO_2 NPs.

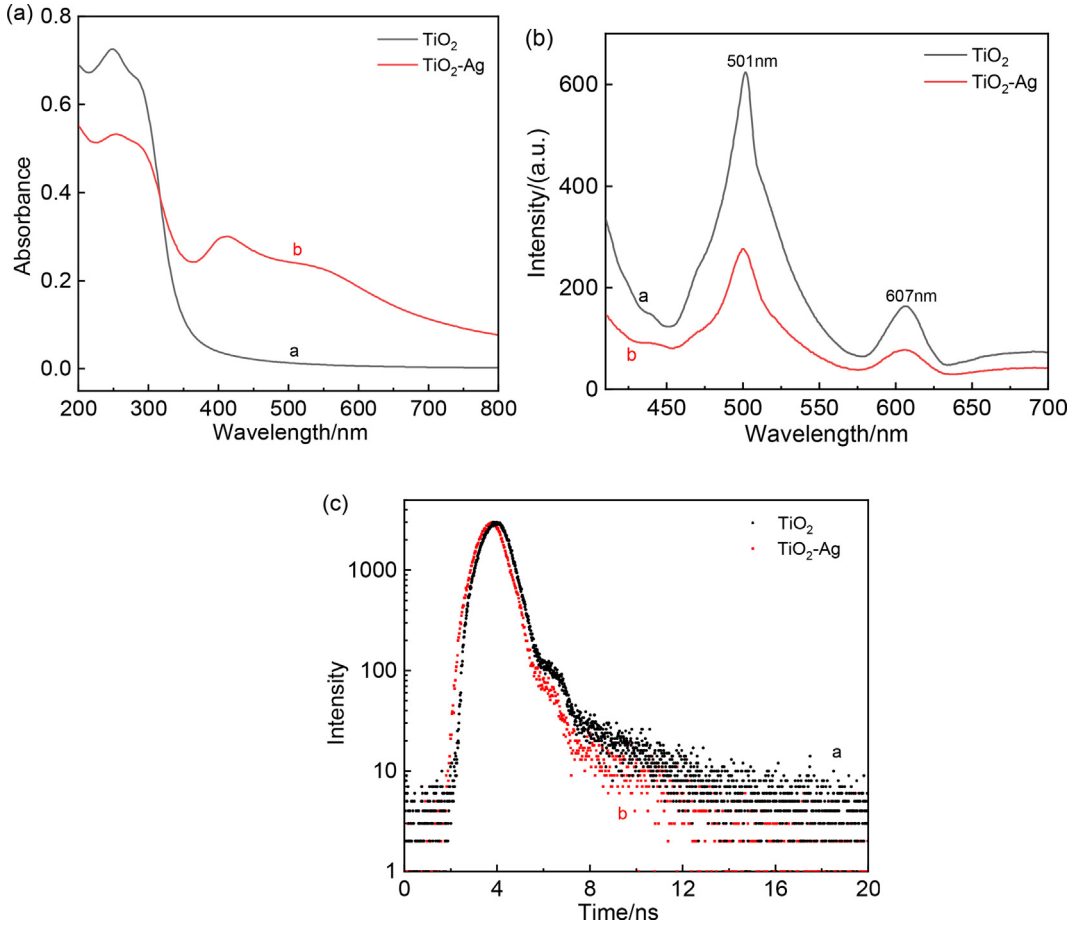

Fig. 4. (a) UV-Vis, (b) PL and (c) TRPL spectra of TiO_2 and Ag-TiO_2 NPs. In the TRPL test, the TiO_2 and Ag-TiO_2 samples were excited at 385 nm and detected at 500 nm.

much lower than those of TiO_2 NPs. It also can be seen from the PL spectra that the peak at 501 nm is higher than 603 nm for both in TiO_2 and Ag-TiO_2 NPs, and the ratio of $Peak_{501}/Peak_{607}$ in TiO_2 is about 3.86. This phenomenon is possibly the result of more trapped holes than trapped electrons in both NPs. The PL intensities of the Ag-TiO_2 NPs decrease in contrast to those of the TiO_2 NPs, and the ratio of $Peak_{501}/Peak_{607}$ also decreases to 3.47. According to the previous results, the loading of Ag NPs results in an increase in the content of surface hydroxyl groups (OH^-), so there is no doubt that the traps formed by the surface OH^- are bound to increase accordingly. The reasons for more surface traps resulting in low PL intensity in the Ag-TiO_2 NPs may be due to the following facts: Firstly, the covering of Ag NPs on TiO_2 may weaken the UV light irradiation onto TiO_2 by scattering or absorption, which would reduce the photogenerated carriers and lower the overall PL activity. Secondly, the conduction band electrons generated by photoexcitation will inject electrons into Ag NPs under UV light irradiation, which may reduce the radiative recombination of TiO_2. Thirdly, the increase of traps may also contribute to non-radiative recombination, which competes with radiative recombination. This also makes the PL intensity decreases. The lower ratio of $Peak_{501}/Peak_{607}$ in Ag-TiO_2 than in TiO_2 indicates that there is more radiative recombination of traps corresponding to the peak at 501 nm in Ag-TiO_2 electrode.

According to the PL results and other previously reported results [19,20], we propose the fluorescence generation mechanism of TiO_2 and Ag-TiO_2 as shown in Fig. 5. Undoubtedly, the fluorescence emissions of TiO_2 and Ag-TiO_2 NPs come from the traps including oxygen vacancies, defects, surface hydroxyl groups, etc. At first, the photo-excitation induced TiO_2 interband transition generates electrons and holes. Then radiative recombination of carriers generates fluorescence, and non-radiative recombination dissipates energy as thermal energy at the interface or bulk. A small portion of uncombined carriers would migrate across the interface and generate photocurrent. The detailed process is given as follows.

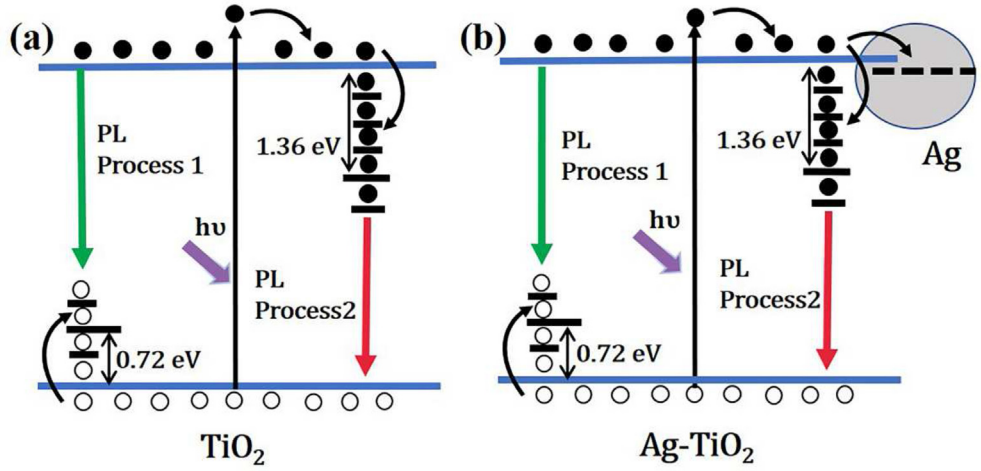

Fig. 5. Schematic diagram of the fluorescence emission mechanism for (a) TiO_2 and (b) Ag-TiO_2 NPs.

1. Charge carriers generation under light excitation:

$$TiO_2 + hv \rightarrow \left(e^-_{CB}\right) + \left(h^+_{VB}\right) \quad (1)$$

2. Carriers trapping by Ti^{4+} or surface OH:

$$\left(e^-_{CB}\right) + TiO_2\left(Ti^{4+}OH\right) \rightarrow TiO_2\left(Ti^{3+}OH\right) \left(\text{trapped electrons}\right) \quad (2)$$

$$\left(e^-_{CB}\right) + TiO_2\left(Ti^{4+}\right) \rightarrow TiO_2\left(Ti^{3+}\right) \left(\text{trapped electrons}\right) \quad (3)$$

$$\left(h^+_{VB}\right) + TiO_2\left(Ti^{4+}OH\right) \rightarrow TiO_2\left(Ti^{4+}O\bullet\right) + H^+ \left(\text{trapped holes}\right) \quad (4)$$

3. Recombination of mobile conduction band electrons with trapped holes.

$$\left(e^-_{CB}\right) + TiO_2\left(Ti^{4+}O\bullet\right) \rightarrow TiO_2\left(Ti^{4+}OH\right) \quad (5)$$

4. Recombination of trapped electrons with mobile valence band holes.

$$\left(h^+_{VB}\right) + TiO_2\left(Ti^{3+}OH\right) \rightarrow TiO_2\left(Ti^{4+}OH\right) \quad (6)$$

$$\left(h^+_{VB}\right) + TiO_2\left(Ti^{3+}\right) \rightarrow TiO_2\left(Ti^{4+}\right) \quad (7)$$

As shown in Fig. 5, the equation (5) is denoted as the process 1, which is the recombination of free electrons in the conduction band (CB) with trapped holes. The fluorescence peak of this process is located at 501 nm, indicating that the maximum density of trapped holes, which can undergo radiative recombination subsequently, is located at 0.72 eV above the valence band (VB) in terms of energy level. In contrast, the equations (6) and (7) are denoted as the process 2, which are the recombination of free holes in VB with trapped electrons [21]. The fluorescence peak of this process is located at 607 nm, indicating the maximum density that can undergo radiative recombination is located at 1.36 eV below CB. Therefore, the trapped electrons are dominated by the deep traps. In other words, the fluorescence emission of the process 2 mainly comes from the recombination process of deep trap states. The reason for the decreased ratio of $Peak_{501}/Peak_{607}$ of Ag-TiO_2 to 3.47 possibly is the increased surface hydroxyl groups mostly acting as electron traps rather than hole traps. The increased electron traps offset part of the process 2 is the electron fluorescence quenching process. Although surface hydroxyl groups can trap both electrons and holes, surface hydroxyl groups act mainly as electron traps in this work.

The lifetime and recombination dynamics of carriers were analyzed by the time-resolved photoluminescence (TRPL) spectrum. The obtained TRPL results and corresponding fitting parameters are given in Fig. 4c and Table S1, respectively. In the TRPL test, the lifetime of carrier was detected at 500 nm corresponding to the process 1. Thus, the process of recombination takes place between conduction band electrons and trapped holes. After loading Ag on the surface of TiO_2, the average carrier lifetime only slightly decreased from 1.79 ns to 1.72 ns. It indicates that the surface hydroxyl groups have a feeble effect on the recombination process of holes and surface hydroxyl groups mainly trap electrons rather than holes. Therefore, the main reason for the fluorescence quenching of the Ag-TiO_2 composite is the weakening of UV light absorption of TiO_2 and the electrons transferring from the TiO_2 conduction band to Ag NPs.

3.3. Electrochemical investigation of traps in TiO_2 and Ag-TiO_2 NPs electrodes

The traps of semiconductor electrodes include surface dangling bonds, adsorbed molecules, surface and bulk defects, etc. Traps can capture carriers, and significantly affect the transfer of electrons and holes at the interface, which has been shown in previous spectroscopic results. To further understand the changes of traps before and after Ag loading, the distribution of traps in TiO_2 and Ag-TiO_2 electrodes at different potentials was investigated by the CA curve. In principle, when the potential was applied to a nano-semiconductor electrode, the Fermi energy level of the electrode is controlled by the applied potential, and the traps around the energy level will be filled with electrons, which are injected from the applied electric field. Therefore, the decay of current in the CA curve is related to the trapping process in the bandgap region [22,23]. The accumulated charge Q can be calculated by integrating the current-time curve from the initial to steady state. The N_{trap} can be calculated by Equation (8).

$$N_{trap(V)} = \frac{1}{q} \times \frac{dQ}{dv} \tag{8}$$

Where, q is the elementary charge, Q is the accumulated charge calculated by integrating, and V is the applied potential. Hence, CA curve provides a direct method to measure the density of traps in electrodes. The CA curves of Ag-TiO_2 and TiO_2 electrodes are shown in Fig. 6a and Fig. S3, respectively. The detailed calculation for the numerical values of Q and traps is given in Table S2.

As seen from Fig. 6a, after the potential stepped from 0.25 V to a negative potential (0.2 to −0.8 V), A sharp cathodic current peak was observed immediately, and then the current decayed to a steady state gradually. Fig. 6b shows the relationship between the Q and the potentials of TiO_2 and Ag-TiO_2 electrodes. It can be seen that both TiO_2 and Ag-TiO_2 electrodes have a low Q at 0.20 V−0 V. As the potential moved to −0.20 V, Q rised almost exponentially. This means that there are a lot of traps at this potential. But this trend slowed down as the potential continued to move negatively. Compared with the TiO_2 electrode, the Ag-TiO_2 electrode has a higher Q, and this also shows that the Ag-TiO_2 electrode has more traps than TiO_2.

As shown in Fig. 6c, the TiO_2 and Ag-TiO_2 electrodes have different trap distributions at different potentials, but both electrodes show a trend of an increase followed by a decrease. The flat band potential and carrier concentration of TiO_2 and Ag-TiO_2 electrodes were examined by the Mott-Schottky plot (Fig. S3). The flat band potentials of TiO_2 and Ag-TiO_2 electrodes are −0.20 V and −0.32 V, respectively. Then the energy level of the conduction band was calculated based on the flat band potential and the carrier concentration. The detailed calculation process is given in S6. For the TiO_2 electrode, $E_C = E_F$+0.10 eV, this means that the conduction band is 0.10 eV above the Fermi level. For the Ag-TiO_2 electrode, $E_C = E_F$+0.091 eV, so the conduction band is 0.091 eV above the Fermi level. Based on this, we draw the traps filling level diagram as shown in Fig. 6d. Since Ag NPs are easily oxidized at positive potentials, the filling depth of the traps is about 0.40−0.50 eV below the conduction band which corresponds to the part of shallow energy levels trapped by surface hydroxyl groups. According to the calculation, in the potential range of 0.20 to −0.60 V the trap density of Ag-TiO_2 electrode is higher than that of TiO_2. The trap density in TiO_2 is $1.47 \times 10^{17}/cm^2$, while $4.14 \times 10^{17}/cm^2$ in Ag-TiO_2, which is about 2.82 times the number of TiO_2. This may be because the Ag-TiO_2 electrode has more surface hydroxyl groups. During the process of the potential step, surface hydroxyl groups can capture injected electrons to generate trapped electrons, which leads to more trap density of the Ag-TiO_2 electrode during measurement. The change of the electrode trap density after Ag loading on TiO_2 will significantly affect the transfer of photogenerated electrons and holes at the interface, and then affects the subsequent photocurrent and photovoltage responses.

3.4. Transient photocurrent of Ag-TiO_2 and TiO_2 NPs electrodes

To investigate the effect of traps on the interfacial charge transfer mechanism of the electrodes, the photocurrent responses of the TiO_2 and Ag-TiO_2 electrodes were measured at 0.2 V under the illumination of different wavelengths (Fig. 7a and b). At this potential, the band bending of TiO_2 is depletion type and Ag will not be oxidized. As shown in Fig. 7a and b, both the TiO_2 and Ag-TiO_2 electrodes exhibited positive photocurrents at all excitation wavelengths. Under continuous light radiation of 365−370 nm, the photocurrent of TiO_2 electrode was raised sharply at first and then slowly increased to a steady state. In contrast, when the excitation wavelength range changed to 385−390 nm, the transient photocurrent exhibited an initial sharp spike and followed by a wide platform with continuous illumination. As the wavelength shifted continuously towards the longer wavelengths, the photocurrent gradually

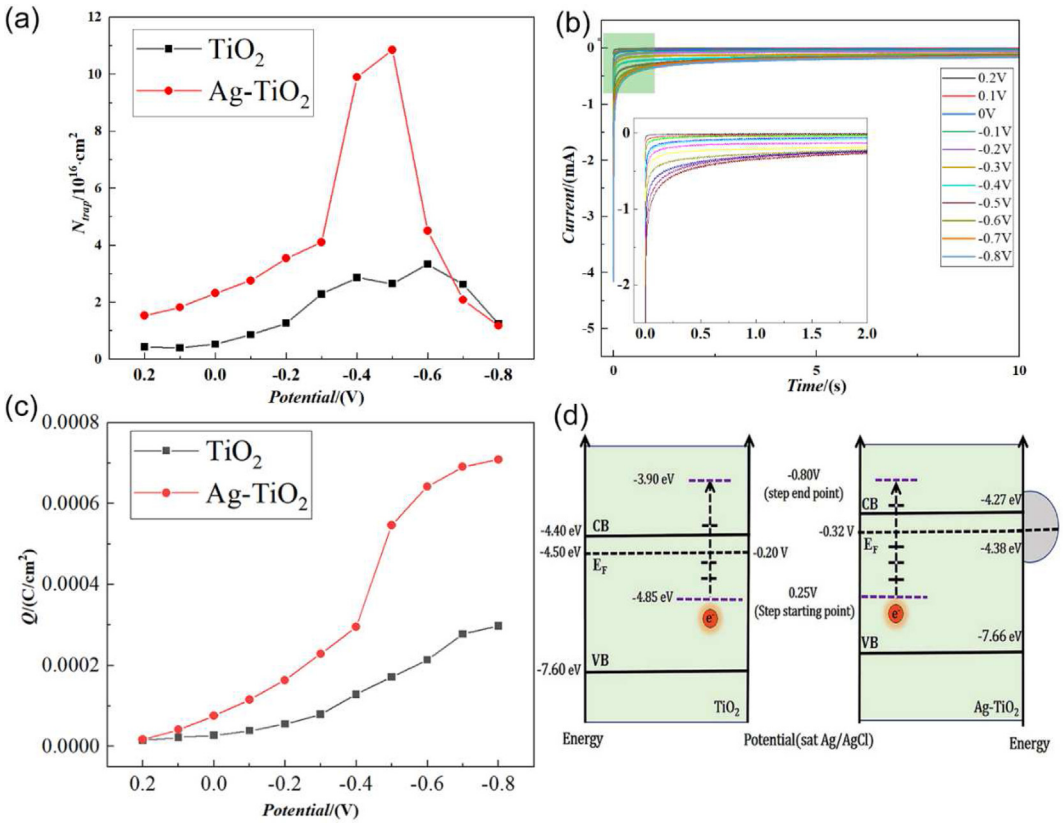

Fig. 6. (a) Chronoamperometric curves of Ag-TiO_2 electrode after the potential step from 0.25 V to different potentials positive of 0.25 V; Accumulated charge density and traps of (b) TiO_2 and (c) Ag-TiO_2 electrodes. (d) The energy band diagram of the trap filling process.

weakened and finally disappeared. In contrast to the varied behavior of TiO_2 electrodes, the Ag-TiO_2 electrodes showed similar transient profiles at different wavelengths. When the light was turned on, a positive current peak appeared and followed by a rapid decay. Inside the visible region, the Ag-TiO_2 electrode still exhibited a high photocurrent response and the photocurrent reached a maximum at 420−430 nm. The difference between the transient behaviors of TiO_2 and Ag-TiO_2 electrodes implies different dynamics. Therefore, the interfacial charge transfer mechanisms under the illumination of two typical wavelengths (UV and Visible light) are discussed based on the results of the transient photocurrent measurements.

The elementary processes of charge transfer under the illumination of UV light on the TiO_2 and Ag-TiO_2 electrodes are schematically illustrated in Fig. 8a and b. The transfer of electrons and holes is the main focus under closed-circuit conditions.

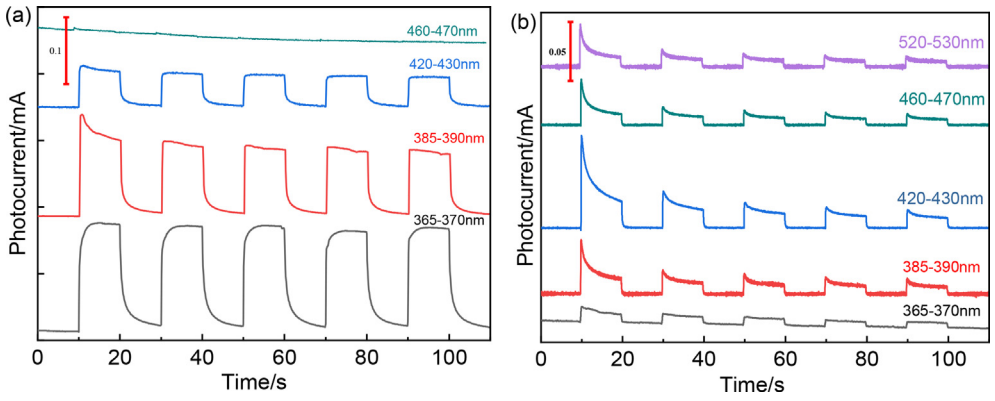

Fig. 7. Transient photocurrent responses of (a) TiO_2 and (b) Ag-TiO_2 electrodes under intermittent light illumination of different excitation wavelengths. The curves were recorded at 0.2 V.

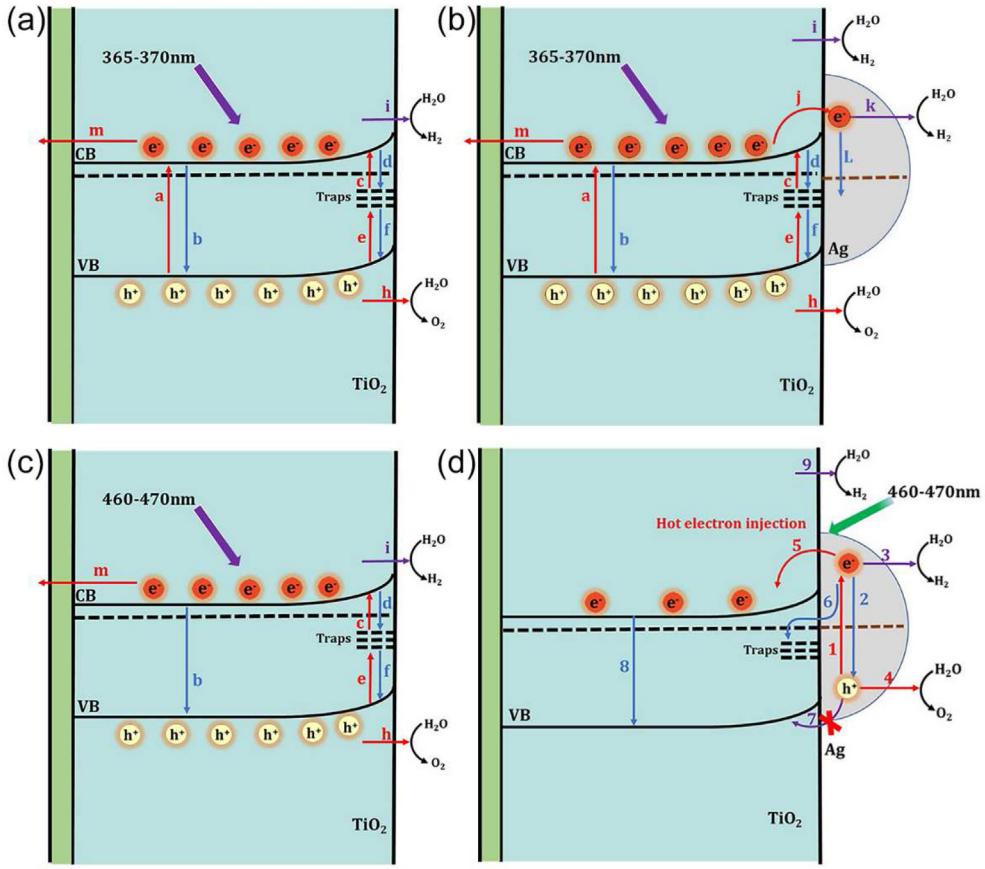

Fig. 8. Mechanisms for charge transfer at the interface of TiO_2 and Ag-TiO_2 electrodes under the illumination of two typical wavelengths. At 365−370 nm (a) TiO_2; (b) Ag-TiO_2; At 460−470 nm (c) TiO_2 (d) Ag-TiO_2; The charge transfer is main focus under closed-circuit conditions.

Process *a* represents the interband excitation of TiO_2, during which a lot of electrons are generated in the conduction band and holes in the valence band. Process *b* is the interband recombination of conduction band electrons and valence band holes. Processes *c* and *e* are the electron transition from the valence band to trap states and from trap states to the conduction band, respectively, which are both trap states related excitations. Processes *d* and *f* are the trap recombination on surface and in bulk, respectively. Processes *i* and *h* are electrons and holes scavenging at the semiconductor/solution interface, respectively. Process *m* is electron transport to the external circuit through FTO. The electron transfer processes between Ag and TiO_2 are accelerated by the loading of Ag onto TiO_2 surface. As shown in Fig. 8b, Process *j* is denoted as the electron transfer from the TiO_2 conduction band to Ag NPs in Ag-TiO_2 and the recombination of carriers process appears on the surface of Ag NPs (Processes *k*, *l*).

At the moment of illumination with 365−370 nm, TiO_2 is almost exclusively excited to generate photogenerated carriers and Processes *a*, *c* and *e* happen first. In the presence of built-in electric field, the photogenerated electrons and holes would be separated. Then the electrons were transferred to the external circuit through FTO (Process *m*), and the holes were transferred to the interface and captured by the redox species (Process *h*) in the solution. Their joint effect leads to a positive photocurrent both in the TiO_2 and Ag-TiO_2 electrodes. As for the TiO_2 electrodes, the number of conduction electrons derived from the interband excitation is far greater than that of trap electrons because the interband excitation (Process *a*) is dominating. Then the electron transition (Process *c*) takes place between shallow trap levels and the conduction band, which is slower than the interband transition. This contributes to the subsequent slight increase of photocurrent. The transient photocurrent response of the Ag-TiO_2 electrode at this wavelength range is different from that of the TiO_2 electrode in two aspects: 1) the steady-state photocurrent is much lower than that of TiO_2; 2) the photocurrent decreases slightly after the initial rise. These differences come from three reasons. First, the deposition of Ag NPs on the TiO_2 surface leads to less light absorption by TiO_2. Second, the Ag-TiO_2 electrodes have more traps

than the pristine TiO_2, increasing the process of trap recombination (Processes *d*, *f*). Finally, the electrons of the conduction band may be transferred to the Ag (Process *j*) and recombined under the irradiation of 365−370 nm light, which induces the decrease of photocurrent.

As the wavelength changed to 385−390 nm, this excitation wavelength range just crosses over the onset wavelength of anatase TiO_2, which means that both interband and intraband excitations occur. In the TiO_2 electrode, shallow trap states also participated in generating carriers along with valence and conduction bands at the moment of illumination, which causes the decreases of conduction electron number and initial photocurrent of 385−390 nm compared with 365−370 nm. Then the transitions from conduction band and shallow traps to deep trap levels came into play, especially the latter. This process led to the subsequent decrease of the photocurrent and the current spike appeared. The shape of photocurrent profile for the Ag-TiO_2 electrode is similar to that of the TiO_2 electrode, but with higher photocurrent spikes. As mentioned in the previous discussion, the increased traps of Ag-TiO_2 and conduction band electrons transferred from TiO_2 to Ag cause the enhancement of recombination, which leads to above photocurrent responses.

As the wavelength shifted to the visible region longer than 470 nm, the Ag-TiO_2 electrode still showed an obvious photocurrent response but the TiO_2 electrode did not. The proposed mechanism of charge transfer at the interfaces of TiO_2 and Ag-TiO_2 is shown in Fig. 8c and d, respectively. Since the TiO_2 electrode exhibited no obvious photocurrent response at this wavelength range, only the excitation of the plasmons of Ag NPs is considered. Process 1 is denoted as the excitation of the plasmons of Ag NPs which generates hot carriers; Process 2 is the immediate hot carriers recombination; Processes 3 and 4 represent the capture of hot holes and hot electrons at the Ag-solution interface, respectively; Process 5 is the hot electron transfer from the Ag NPs to the conduction band of the TiO_2 NPs at this wavelength; Process 6 is the recombination of the hot electrons with traps. After electrons were transferred to the TiO_2 through Process 5, Processes 8 and 9 took place. Process 8 corresponds to the interband recombination at the TiO_2. Process 9 is the hot electrons captured by water at the TiO_2 surface. For the TiO_2 electrode, in the wavelength range of 460−470 nm, the energy of incident photons is so low that only little traps were excited. In addition to partial recombination e^-/h^+ pairs, the number of carriers forming the current is too small to detect obvious photocurrent. But the Ag-TiO_2 electrode exhibits maximum photocurrent at 420−430 nm, which corresponds to the SPR absorption peak of Ag NPs. At the beginning of illumination, the plasmons of Ag NPs were excited to generate lots of hot carriers (Process 1). Part of the high-energy electrons crossed the barrier and were transferred to the conduction band of the TiO_2 (Process 5) then to the external circuit along the conduction band. Apart from this, the electrons and holes were also transferred to the Ag-solution interface and captured by the redox species, which generated negative and positive currents, respectively. But the net results of these processes show that the anodic process is faster than the cathodic process, which leads to a positive photocurrent. As the illumination continues, the carriers were rapidly accumulated, causing the enhanced recombination (Processes 2 and 6). This is reflected by the decay and spike of the photocurrent. But at this point the positive process still dominates, so the net result of the photocurrent is still positive.

Under the irradiation of the UV region, the Ag-TiO_2 electrode has a weaker photocurrent but more obvious spike than the pristine TiO_2 electrode. Both the intensity and trend of photocurrent indicate more carriers recombination process in the Ag-TiO_2 electrode. Therefore, the recombination of the electrodes at different wavelengths is quantitatively estimated by fitting the photocurrent decay curves [24]. The photocurrent decay curves of the electrode at different wavelengths can be generally divided into three segments as shown in Fig. 9: (1) the photocurrent spikes at the instant of illumination with a current value of J_0; (2) the photocurrent decays toward a steady-state value of J_∞ and (3) the photocurrent rapidly decays to 0 at the instant of light cutoff.

At the instant of illumination, the electron-hole occurs and leads to the generation of positive

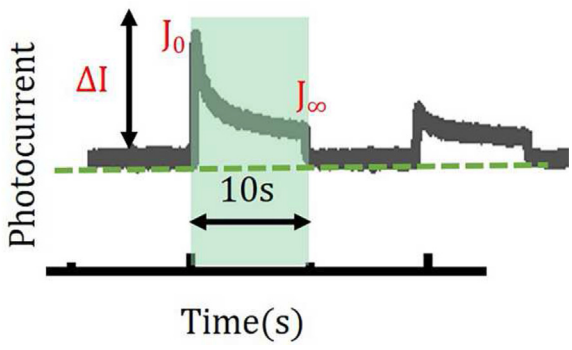

Fig. 9. Photocurrent transients of TiO_2 and Ag-TiO_2 electrodes. Where J_0 represents the photocurrent peak measured at $t \approx 0$, and J_∞ was measured at $t = 10$ s.

photocurrent. As the illumination continues, the recombination at the surface and bulk increases, and the strong recombination results in a positive photocurrent spike. Under prolonged light illumination, the carriers recombination reached a steady state, thus the photocurrent gradually achieves a steady state too. Based on this, Equation (9) can be derived

$$\frac{J_\infty}{J_o}=\frac{k_{tr}}{k_{tr}+k_{rec}} \tag{9}$$

Where, k_{rec} is the carriers recombination rate constant and k_{tr} is the carriers charge transfer rate constant at the semiconductor-electrolyte interface. The carriers transfer and recombining kinetic constants $R_{t/r} = k_{tr}/k_{rec}$ for the TiO_2 and Ag-TiO_2 electrodes at different wavelengths are calculated and the results are shown in Table 1. According to the results, the values of interfacial charge transfer coefficient $R_{t/r}$ for the Ag-TiO_2 electrode are less than 1 at all wavelengths, which implies that the number of recombined photogenerated carriers in the Ag-TiO_2 electrode under light is larger than that of transferred ones. Furthermore, the charge transfer coefficient $R_{t/r}$ of the Ag-TiO_2 electrode gradually decreases with the red-shift of wavelength, which is due to the energy of hot electrons generated by the SPR excitation of Ag decreased. Hot electrons are harder to cross the Schottky barrier causing the increased recombination. In addition, the values of interfacial charge transfer coefficient of $R_{t/r}$ for the Ag-TiO_2 electrode are smaller than that of the pristine TiO_2, indicating a stronger charge recombination process in the Ag-TiO_2 electrode. In the previous calculation of trap state in Section 3.3, the trap state densities of Ag-TiO_2 electrodes are much higher than those of TiO_2. The higher density of deep traps may lead to the increase in the nonradiative recombination of carriers and inhibit the interfacial carrier transfer. This is also the reason for the TiO_2 electrode maintaining a relatively stable photocurrent during multiple light on-off cycles, while the Ag-TiO_2 electrode has a gradually decreasing transient photocurrent response. The photo-generation, transfer, recombination and other processes of carriers often need to go through several intermittent cycles before achieving an equilibrium, and this is closely related to trap states. The more traps the electrode has, the longer time it takes to reach stable state. On the other hand, the injection of photogenerated electrons from TiO_2 to Ag is another major reason for the decrease of $R_{t/r}$ for the Ag-TiO_2 electrode in the UV region. After loading Ag on the TiO_2 surface, part of the photogenerated electrons may be transferred to the Ag and annihilated under the illumination of UV light, which has been confirmed by photoluminescence spectroscopy. Thus, the two main reasons result in a reduced photocurrent response in the UV region in this system.

Table 1. K_{tr}/K_{rec} at different wavelengths for theTiO_2 and Ag-TiO_2 electrodes.

Wavelength/nm	K_{tr}/K_{rec}	
	TiO_2	Ag-TiO_2
365−370	−2.51	0.97
385−390	2.85	0.47
420−430	6.14	0.45
460−470	/	0.38
520−530	/	0.35

Consequently, the photocurrent curves of TiO_2 and Ag-TiO_2 electrodes were recorded, accordingly, the photocurrent shape and intensity are analyzed in this part. The existence of Processes 5 and *j* indicates that the direction of interfacial charge transfer in Ag-TiO_2 is different at different wavelengths. Under UV illumination, electrons are transferred from TiO_2 to the surface of Ag. On the contrary, under visible light, hot electrons cross the barrier and are transferred from Ag to TiO_2. Therefore, the molecular reactions taking place at the Ag surface can be modulated easily by changing light wavelengths. Additionally, the charge transfer/recombination ratios of TiO_2 and Ag-TiO_2 electrodes at different wavelengths can be calculated. The result shows that there is more carrier recombination in the Ag-TiO_2 electrode than that in the TiO_2 electrode. Combining the results of Section 3.3, part of the increased surface hydroxyl groups may act as deep trap states, inhibiting the separation of carriers and increasing the recombination process. This means that we should control the number of traps for better SPR catalytic performance.

3.5. Transient photopotential and photogenerated electron-hole recombination processes at Ag-TiO_2 interface

To further investigate the photogenerated electron-hole recombination processes at the Ag-TiO_2 interface, the open circuit photopotential responses of TiO_2 and Ag-TiO_2 electrodes had been measured under the irradiation of different wavelengths. As shown in Fig. 10a and b, the OCPs of both TiO_2 and Ag-TiO_2 electrodes moved negatively when illuminated, which is a typical n-type semiconductor characteristic. Under UV light irradiation, the Ag-TiO_2 electrodes exhibited weaker photopotential responses than the TiO_2

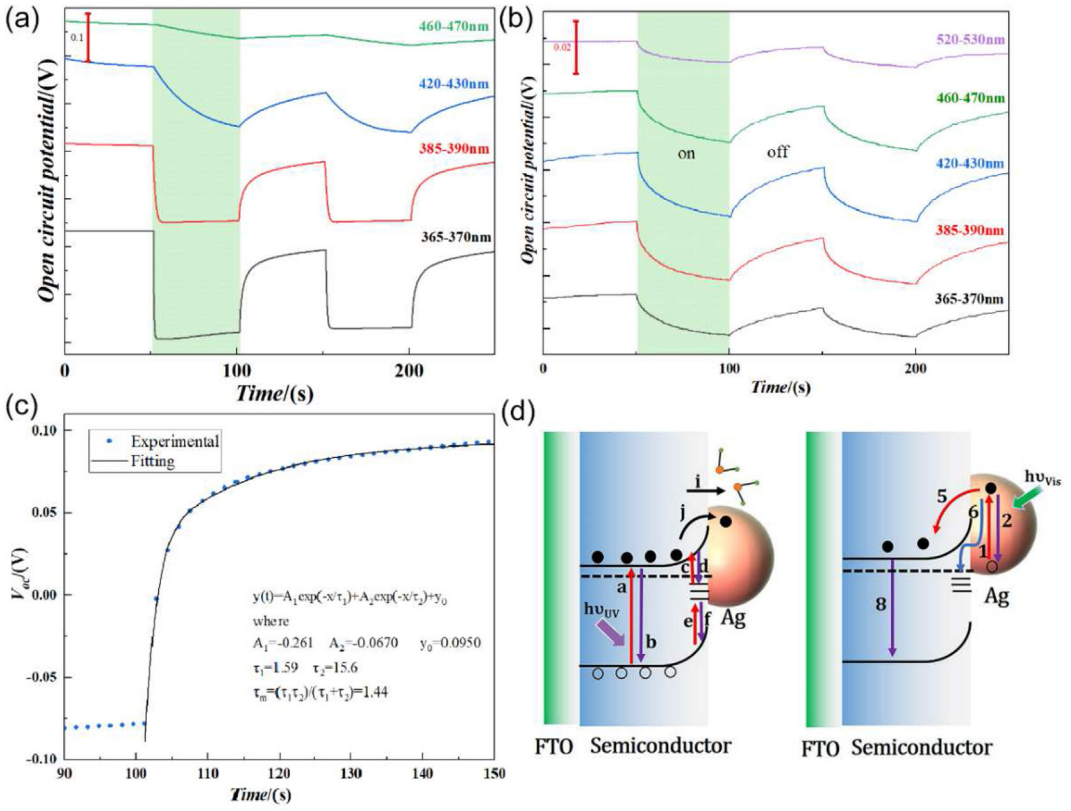

Fig. 10. Transient photopotential responses at different wavelengths under intermittent illumination. (a) TiO_2 and (b) Ag-TiO_2 electrodes; (c) double exponential fitting curves of photopotential decay for TiO_2 after irradiation at 360−370 nm. (d) The mechanisms of interfacial charge recombination of Ag-TiO_2; left is 365−370 nm; right is 460−470 nm. Here, the recombination of photogenerated carriers is the main process under open circuit condition.

electrodes. But the Ag-TiO_2 electrodes still had obvious photopotential response under the irradiation of visible light until 520−530 nm light, while the TiO_2 electrodes had almost no response at longer wavelengths than 420−430 nm.

The mechanisms of interfacial charge recombination on the TiO_2 and Ag-TiO_2 electrodes are shown in Fig. 10d. Since there is no current in the circuit under open circuit conditions, it is the photogenerated carrier accumulated on surfaces that led to the OCP shift of electrodes. Then the electrons and holes are forced to recombine, which leads to the decay of the transient photopotential. For the TiO_2 and Ag-TiO_2 electrodes, the electrons were accumulated in the conduction band at the moment of illumination, which causes the Fermi level to move upward [25]. Therefore, both the TiO_2 and Ag-TiO_2 electrodes show a negative OCP shift under the irradiation. However, the Ag-TiO_2 electrodes had a weaker photopotential response than the TiO_2 electrodes in the UV region. This phenomenon mainly comes from the following points: (a) the covering effect of Ag on TiO_2 may weaken part of UV light irradiation; (b) the charge transfer from TiO_2 to Ag NPs (Process *j*) under UV light irradiation partially removes the accumulated electrons; (c) the Ag-TiO_2 electrode had a higher trap density than the TiO_2 electrode, which may capture photo-induced carriers and recombination (Process *i*), and then lead to less accumulated interfacial charges and lower photopotential.

The decay rate of photopotential after the illumination cutoff is a good indication of electrode trap states. The recombination kinetics of accumulated interfacial carriers can be extracted from decay profiles after the illumination cutoff [26]. The decay profiles of TiO_2 and Ag-TiO_2 electrodes under the illumination of different wavelengths are fitted using a bi-exponential model:

$$y(t) = A_0 + A_1\, exp(-t/\tau_1) + A_2\, exp(-t/\tau_2) \quad (10)$$

$$\tau_m = (\tau_1\tau_2)/(\tau_1+\tau_2) \quad (11)$$

Where τ_1 and τ_2 are the carrier lifetimes, τ_m is the harmonic mean lifetime, A_1 and A_2 are the corresponding pre-exponential factors. Fig. 10c shows the photopotential decay fitting and lifetime calculation of TiO_2 electrode under 365−370 nm illumination. The fitting results from Fig. 10 are shown in Table 2. More fitting results at other

Table 2. Calculation of decay lifetime by photopotentials of TiO_2 and Ag-TiO_2.

Wavelength/nm	Sample	A_1	τ_1/s	A_2	τ_2/s	τ_m/s
365−370	TiO_2	−0.261	1.59	−0.067	15.60	1.44
	Ag-TiO_2	−0.0009	2.51	−0.012	36.84	2.34
460−470	TiO_2	−0.015	5.82	−0.083	38.89	5.06
	Ag-TiO_2	-2.930×10^{-3}	4.229	-1.415×10^{-2}	30.84	3.72
	Ag	−0.006	2.85	−0.005	29.34	2.59

wavelengths are shown in S5 and S6. The calculated carrier lifetime values of TiO_2 and Ag-TiO_2 electrodes are mostly in the range of several seconds, which is comparable to the time scale of interfacial reactions. Therefore, this method mainly focuses on the interface charge transfer process after contact with the solution.

The fitting results show that the photopotential decay of TiO_2 electrodes at 365−370 nm can be divided into a fast process and a slow process. At this wavelength, the excitation is mostly from the interband transition of TiO_2. Because the interband recombination is much faster than trap recombination, the fast part corresponds to the interband recombination (Process *b*) and the slow part can be attributed to the recombination of traps like surface hydroxyl groups and solution species (Processes *d* and *i*). Similar to the TiO_2 electrode, the fast decay after cutoff of Ag-TiO_2 electrode can be ascribed to the interband recombination, too. The slow decay mainly corresponds to trap recombination, and partially to electron transfer toward the Ag. As shown in Fig. 10a and b, the slope of the photopotential decay curve for the TiO_2 electrode is much higher than that of the Ag-TiO_2 at 365−375 nm. The sharp curves indicate that the fast process has a large contribution to the total photopotential response. Hence the ratio of the slow recombination process in the Ag-TiO_2 electrode is significantly higher compared with that in the TiO_2 electrode. It is the result of increased hydroxyl of Ag-TiO_2 NPs, compared with that of TiO_2 electrodes, the Ag-TiO_2 electrodes have more shallow traps recombination process. Another contributing factor is the charge transfer from TiO_2 to Ag (Process *j*) at this wavelength, which also helps separate electron-hole pairs and induces the slow process to be increased. The increase of the slow recombination process may results in a prolonged carrier lifetime [27], so the carrier lifetime of Ag-TiO_2 is longer than that of TiO_2 at this wavelength.

As the excitation wavelength is shifted toward longer wavelengths, the slope of the decay curves for the TiO_2 electrode decreases accordingly. Under sub-band illumination, the photon energy is not high enough to excite the interband transition, thus fewer and fewer electrons are excited to the conduction band (Process *a*). In this condition, electrons are excited to shallow traps (Process *e*). Few electrons can be transferred to the conduction band (Process *c*) and recombination with holes. Therefore, trap recombination processes gradually dominate. The increased slow process contributes to lower slopes and longer carrier lifetime. Under the illumination of 460−470 nm, only trap states can be excited and few electrons could be transferred to the conduction band. The fitting result is monoexponential, which means only slow process happens at this wavelength, and the calculated photogenerated carrier lifetime is also increased to 59.75s.

For the Ag-TiO_2 electrode, the excitations are mostly from the SPR of Ag NPs under 460−470 nm and longer wavelengths. Due to the lifetime of hot carriers generated by plasmonic relaxation is relatively short, the fast process in the photopotential decay after cutoff can be attributed to the interband recombination in TiO_2 and the slow decay mainly corresponds to the recombination of traps in TiO_2. These processes happened after hot electrons being transferred across the energy barrier from Ag toward the TiO_2 conduction band. There are more traps but a shorter carrier lifetime in the Ag-TiO_2 electrode. The results of which indicate that hot electrons in Ag are more likely to be recombined with deep traps at the interface (Process 6) than transferred to the conduction band of the TiO_2 (Process 5). In this case, the lower excitation energy is more beneficial to the recombination process of hot electrons with deep traps, which leads to the decrease of the R_{tr}/R_{rec} ratio as the wavelength shifts toward the longer one. Furthermore, the transient photopotential of Ag NPs was also measured for comparison, as shown in Fig. S7. The Ag-TiO_2 electrode has a higher photopotential and a longer lifetime compared with the Ag electrode. Because the Schottky barrier at the Ag-TiO_2 interface can effectively separate the charge carriers (Process 5), thereby the carrier lifetime is prolonged.

4. Conclusions

In summary, the effects of traps on the photoinduced interfacial charge transfer of Ag-TiO_2 were systematically investigated by using photoelectrochemical, electrochemical, and spectroscopic

methods. Trap state densities of TiO_2 and Ag-TiO_2 were evaluated by PL measurements and the distributions of traps in the TiO_2 and Ag-TiO_2 electrodes at different potentials were estimated by potential step CA measurements. In comparison with the TiO_2 electrode, the trap density of the Ag-TiO_2 electrode was found to be significantly higher. According to the IR and XPS characterizations, the increase of traps may be attributed to the increase of hydroxyl groups on the surface of TiO_2 in the composite, and the traps mainly act as electrons trap rather than holes trap in the as-synthesized Ag-TiO_2 of this work. The charge transfer/recombination ratios, which were determined by the transient photocurrent measurements, show that there were more carrier recombination in the Ag-TiO_2 electrode than in the TiO_2 electrode. The increased traps, including deep and shallow traps, reduced the photocurrent in the UV region. On the other side, the comparison of the photogenerated carrier lifetime for the TiO_2 and Ag-TiO_2 electrodes, which were estimated through the transient photopotential measurements, indicates that the increased traps promoted the recombination process but prolonged the lifetime of carriers. This possibly can be attributed to the transitions among the conduction band, shallow trap states and deep trap states. The shallow traps may capture photoexcited electrons and transfer the carriers to the conduction band for reuse. These results emphasize the roles of different kinds of traps in metal-semiconductor composite, which should be considered to get a better catalytic activity or modulate the reaction taking place on the Ag interface. Meanwhile, the combined utilization of photoelectrochemical, electrochemical and spectroscopic methods in this work also broadens the research methods of the plasmonic composite system and provides a reference for the in-depth study of metal-semiconductor composite.

Acknowledgments

The authors acknowledge supports from the National Natural Science Foundation of China (No. 22032004) and the Ministry of Science and Technology of China (No. 218YFC1602805).

References

[1] Zhan C, Chen X J, Yi J, Li J F, Wu D Y, Tian Z Q. From plasmon-enhanced molecular spectroscopy to plasmon-mediated chemical reactions[J]. Nat. Rev. Chem., 2018, 2(9): 216−230.

[2] Zhang Y C, He S, Guo W X, Hu Y, Huang J W, Mulcahy J R, Wei W D. Surface-plasmon-driven hot electron photochemistry[J]. Chem. Rev., 2018, 118(6): 2927−2954.

[3] Gelle A, Jin T, de la Garza L, Price G D, Besteiro L V, Moores A. Applications of plasmon-enhanced nanocatalysis to organic transformations[J]. Chem. Rev., 2020, 120(2): 986−1041.

[4] Brongersma M L, Halas N J, Nordlander P. Plasmon-induced hot carrier science and technology[J]. Nat. Nanotechnol., 2015, 10(1): 25−34.

[5] Moon C W, Choi M J, Hyun J K, Jang H W. Enhancing photoelectrochemical water splitting with plasmonic Au nanoparticles[J]. Nanoscale Adv, 2021, 3(21): 5981−6006.

[6] Ingram D B, Linic S. Water splitting on composite plasmonic-metal/semiconductor photoelectrodes: evidence for selective plasmon-induced formation of charge carriers near the semiconductor surface[J]. J. Am. Chem. Soc., 2011, 133(14): 5202−5205.

[7] Wang S J, Zhang X Y, Su D, Yan X, Zhou H L, Xue X M, Wang Y F, Zhang T. Enhanced photocatalytic reactions via plasmonic metal-semiconductor heterostructures combing with solid-liquid-gas interfaces[J]. Appl. Catal. B-Environ., 2022, 306: 121102.

[8] Kim Y, Creel E B, Corson E R, McCloskey B D, Urban J J, Kostecki R. Surface-plasmon-assisted photoelectrochemical reduction of CO_2 and NO_3^- on nanostructured silver electrodes[J]. Adv. Energy Mater., 2018, 8(22): 1800363.

[9] Huang H N, Shi R, Li Z H, Zhao J Q, Su C L, Zhang T R. Triphase photocatalytic CO_2 reduction over silver-decorated titanium oxide at a gas-water boundary[J]. Angew. Chem. Int. Ed., 2022, 61(17): e202200802.

[10] Saravanan R, Manoj D, Qin J Q, Naushad M, Gracia F, Lee A F, Khan M M, Gracia-Pinilla M A. Mechanothermal synthesis of Ag/TiO_2 for photocatalytic methyl orange degradation and hydrogen production[J]. Process Saf. Enivron. Protect., 2018, 120: 339−347.

[11] Christopher P, Ingram D B, Linic S. Enhancing photochemical activity of semiconductor nanoparticles with optically active Ag nanostructures: photochemistry mediated by Ag surface plasmons[J]. J. Phys. Chem. C, 2010, 114(19): 9173−9177.

[12] Furube A, Du L, Hara K, Katoh R, Tachiya M. Ultrafast plasmon-induced electron transfer from gold nanodots into TiO_2 nanoparticles[J]. J. Am. Chem. Soc., 2007, 129(48): 14852−14853.

[13] Zhang Y C, Guo W X, Zhang Y L, Wei W D. Plasmonic photoelectrochemistry: in view of hot carriers[J]. Adv. Mater., 2021, 33(46): 2006654.

[14] Ichinose H, Terasaki M, Katsuki H. Properties of peroxotitanium acid solution and peroxo-modified anatase sol derived from peroxotitanium hydrate[J]. J. Sol-Gel Sci. Technol., 2001, 22(1−2): 33−40.

[15] Damato T C, de Oliveira C CS, Ando R A, Camargo P HC. A facile approach to TiO_2 colloidal spheres decorated with Au nanoparticles displaying well-defined sizes and uniform dispersion[J]. Langmuir, 2013, 29(5): 1642−1649.

[16] Yang L B, Jiang X, Ruan W D, Yang J X, Zhao B, Xu W Q, Lombardi J R. Charge-transfer-induced surface-enhanced Raman scattering on Ag-TiO_2 nanocomposites[J]. J. Phys. Chem. C, 2009, 113(36): 16226−16231.

[17] Zhang Y, Chen J R, Tang H, Xiao Y G, Qiu S F, Li S J, Cao S S. Hierarchically-structured SiO_2-Ag@TiO_2 hollow spheres with excellent photocatalytic activity and recyclability[J]. J. Hazard. Mater., 2018, 354: 17−26.

[18] Hong D C, Lyu L M, Koga K, Shimoyama Y, Kon Y. Plasmonic Ag@TiO_2 core-shell nanoparticles for enhanced CO_2 photoconversion to CH_4[J]. ACS Sustain. Chem. Eng., 2019, 7(23): 18955−18964.

[19] Kohtani S, Kawashima A, Miyabe H. Reactivity of trapped and accumulated electrons in titanium dioxide photocatalysis[J]. Catalysts, 2017, 7(10): 303.

[20] Zhang L W, Mohamed H H, Dillert R, Bahnemann D. Kinetics and mechanisms of charge transfer processes in

photocatalytic systems: a review[J]. J. Photochem. Photobiol. C-Photochem. Rev., 2012, 13(4): 263−276.
[21] Mercado C, Seeley Z, Bandyopadhyay A, Bose S, McHale J L. Photoluminescence of dense nanocrystalline titanium dioxide thin films: effect of doping and thickness and relation to gas sensing[J]. ACS Appl. Mater. Interfaces, 2011, 3(7): 2281−2288.
[22] Wang H L, He J J, Boschloo G, Lindström H, Hagfeldt A, Lindquist S E. Electrochemical investigation of traps in a nanostructured TiO_2 film[J]. J. Phys. Chem. B, 2001, 105(13): 2529−2533.
[23] Naseri N, Kim H, Choi W, Moshfegh A Z. Optimal Ag concentration for H_2 production via Ag: TiO_2 nanocomposite thin film photoanode[J]. Int. J. Hydrog. Energy, 2012, 37(4): 3056−3065.
[24] Hernández S, Gerardi G, Bejtka K, Fina A, Russo N. Evaluation of the charge transfer kinetics of spin-coated $BiVO_4$ thin films for sun-driven water photoelectrolysis[J]. Appl. Catal. B, 2016, 190: 66−74.
[25] DuChene J S, Sweeny B C, Johnston-Peck A C, Su D, Stach E A, Wei W D. Prolonged hot electron dynamics in plasmonic-metal/semiconductor heterostructures with implications for solar photocatalysis[J]. Angew. Chem. Int. Ed., 2014, 53(30): 7887−7891.
[26] Moon S Y, Song H C, Gwag E H, Nedrygailov I I, Lee C, Kim J J, Doh W H, Park J Y. Plasmonic hot carrier-driven oxygen evolution reaction on Au nanoparticles/TiO_2 nanotube arrays[J]. Nanoscale, 2018, 10(47): 22180−22188.
[27] Moser J E. Perovskite photovoltaics: slow recombination unveiled[J]. Nat. Mater, 2017, 16(1): 4−6.

陷阱态对 Ag-TiO_2 光诱导界面电荷转移的影响：电化学、光电化学和光谱表征

梁志豪，王家正，王丹，周剑章*，吴德印
厦门大学化学化工学院，固体表面物理化学国家重点实验室，福建 厦门 361005

摘要

在基于金属-半导体异质结构的等离激元介导化学反应中，了解其中的电荷转移和复合机制进而调控界面、提高界面电荷分离，对于提高等离激元催化反应效率至关重要。但电化学体系中固液界面上的等离激元光电催化反应是一个多过程、多时间尺度、多影响因素的复杂体系，光生载流子在界面间传递机制的研究仍面临着巨大的挑战。由于光电化学信号的产生和变化包含了诸多体相和界面过程，因此光电化学方法是探究等离激元催化反应过程中的界面电荷转移机制的有效手段之一。本文合成了 TiO_2 和 Ag-TiO_2 纳米粒子，以光电化学方法作为主要研究手段，并结合电化学和各种谱学表征手段，探究了电极陷阱态对界面电荷转移机制的影响。结果表明，在 Ag 负载在 TiO_2 表面后，电极的陷阱态显著增加。结合 XPS 以及 PL 光谱，陷阱态增加可主要归咎于表面羟基。陷阱态的增加导致了荧光的猝灭和光电响应的减弱，但增加的陷阱态复合过程也延长了载流子的寿命。陷阱态的调控必然会影响界面电荷转移，从而改变热载流子的数量和寿命，进而调控后续 Ag 界面上的等离激元反应。在反应位点位于金属的基于金属-半导体复合体系的等离激元催化反应中，认识到半导体陷阱态对于界面电荷转移的作用有助于在等离激元介导化学反应中更好地利用载流子、提高反应效率。

关键词：等离激元；Ag-TiO_2；陷阱态；电荷转移；光电化学表征